Available online at www.sciencedirect.com
ScienceDirect
Journal of Catalysis 243 (2006) 410–419
JOURNAL OF CATALYSIS
www.elsevier.com/locate/jcat

Catalytic oxidation of cycloolefins over Co(cyclam)-functionalized SBA-15 material with H_2O_2

Sujandi [a], Sang-Cheol Han [a], Dae-Soo Han [a], Myung-Jong Jin [b], Sang-Eon Park [a,*]

[a] *Laboratory of Nano-Green Catalysis, Department of Chemistry, Inha University, 253 Yonghyun-dong, Nam-gu, Incheon 402-751, Republic of Korea*
[b] *Department of Chemical Engineering, Inha University, 253 Yonghyun-dong, Nam-gu, Incheon 402-751, Republic of Korea*

Received 21 February 2006; revised 30 July 2006; accepted 3 August 2006

Abstract

Cobalt in the form of a Co(III) complex was successfully anchored on a cyclam-tethered SBA-15, which was synthesized from a chemical modification of chloropropyl-functionalized SBA-15 and proved to be a selective catalyst for the allylic oxidation of cycloolefins, such as cyclopentene, cyclohexene, and cycloheptene with hydrogen peroxide. The Co(III)-SBA-15 showed high selectivity for the corresponding allylic hydroperoxides, which exceeded 50% after a 12-h reaction time. We conclude that the cobalt species underwent reversible redox cycles, and the formation of cobalt hydroperoxo species derived from the activation of the Co(III) complex with H_2O_2 was attributed to the high selectivity for hydroperoxides as major products. The reversible redox cycle between the Co(III) and Co(II) couple during the oxidation of cycloolefins was supported by a cyclic voltammetry analysis.

Keywords: Co(III); SBA-15; Heterogeneous; Oxidation; Cycloolefin; H_2O_2; Allylic hydroperoxide

1. Introduction

Ordered mesoporous materials have opened many new possibilities for applications in the fields of heterogeneous catalysis, adsorption, and separation because of their large and well defined pore sizes and high surface areas [1–4]. Owing to the inert nature of silica surface, mesoporous materials have suffered from lack of active sites, which are necessary for practical applications, especially in catalysis [1–3]. Functionalization of catalytic homogeneous system has been widely applied in recent years for generating active sites onto the mesoporous silica surfaces [5]. Numerous strategies have been described for immobilizing inorganic and/or organic active species within the silica matrices [5]. The active species could be immobilized either onto the framework through isomorphous substitution of silica [1,2,6–8] or by filling the void space in the pore via a tethering group [1,2,9]. Only a few metallic species can be incorporated into the silica walls, due to difficulties in the formation of metal–O–Si bonds [7,8]. Moreover, only part of the framework metals located on the surface is accessible and catalytically active. In contrast, grafting with a tethering functional group onto the surface provides a wider variety of active species to be anchored in the easily accessible void space of the pores [9,10]. The functionality through tethering can also be tailored by design for the intended catalytic reaction, such as base, acid, and redox-catalyzed reactions [11].

Functionalization of mesoporous silica surface by the immobilization of active sites via a tethering group generally can be done in two different ways: through the so-called "postsynthesis" method, which involves grafting an organotrialkoxysilane onto the pore surfaces after mesoporous material synthesis, and through the direct synthesis method, in which the functional groups are introduced during the gel formation. The pore functionalizations are generated from the co-condensation reaction between the organotrialkoxysilane and silica source in the presence of a structure-directing agent [12]. The direct synthesis method is considered more plausible, because it can avoid several shortcomings of the postgrafting method, such as reduction in pore size, pore blocking at the aperture, and difficulties in

* Corresponding author.
E-mail address: separk@inha.ac.kr (S.-E. Park).

0021-9517/$ – see front matter
doi:10.1016/j.jcat.2006.08.010

controlling the loadings as well as distributions of the active sites [13].

Cobalt salts and their complexes have been widely used as homogeneous catalysts for the oxidation of organic substrates in organic syntheses as well as in the chemical industry. Co(III) has been found to be the catalytically active species in many oxidation reactions [14–16]. Hence, for practical applications, catalytic systems that can accelerate the oxidation of Co(II) to Co(III) and stabilize the Co(III) state are required [17]. Das and Clark [15] and Park et al. [16] immobilized Co(III) onto carboxylic group-tethered HMS and SBA-15 mesoporous silica and found that in these heterogeneous systems, the cobalt cation was weekly bound to the carboxylic group and the tethering of Co(III) for support occurred only on addition of pyridine. Even when pyridine was used to stabilize the Co(III) species, the catalyst was still easily deactivated during the catalytic reaction due to the loss of pyridine. To overcome this problem, the challenge is to find a ligand that can provide a stable environment and stabilize the high-valent metal centers.

In the present work, we immobilized Co(III) species onto SBA-15 in the form of Co(III)cyclam complex, which was covalently tethered onto the SBA-15 surface via the propyl group. Cyclam was chosen because it is a well-known tetraazamacrocycle ligand that can form and stabilize various high-valent transition metal complexes [18]. The cyclam was tethered onto the SBA-15 surface through the substitution reaction of the chloro group of chloropropyl-functionalized SBA-15 (Clpr-SBA-15), which was synthesized using a microwave-assisted direct synthesis method. The formation of the Co(III)cyclam complex was done through the metallation of the tethered cyclam with Co(II) and subsequent aerial oxidation of the Co(II)cyclam to Co(III)cyclam complex [19,20]. The catalytic behavior of the obtained Co(III)cyclam-functionalized SBA-15 [Co(III)-SBA-15] was investigated for the liquid-phase catalytic oxidation of cycloolefins with aqueous hydrogen peroxide (35%). It was shown that the Co(III)-SBA-15 catalyzed the cycloolefin oxidation via allylic substitution mechanism, yielding the corresponding allylic hydroperoxides as major products.

2. Experimental

2.1. Chemicals

Sodium metasilicate ($Na_2SiO_3 \cdot 9H_2O$; Sigma Aldrich) and 3-chloropropyl triethoxysilane/CPTS ($Cl(CH_2)_3Si(OEt)_3$; Aldrich) were used as silica and chloropropyl group sources, respectively. A Pluronic P123 triblock copolymer (poly(ethylene oxide)–poly(propylene oxide)–poly(ethylene oxide)/$EO_{20}PO_{70}EO_{20}$; MW5800; BASF), was used as a structure-directing agent. $CoCl_2 \cdot 6H_2O$, cyclopentene, cyclohexene, cycloheptene, and HPLC-grade acetonitrile solvent were purchased from Aldrich. The tetraazamacrocycle (cyclam) was synthesized according to the following procedure. Nickel(II) perchlorate hexahydrate, 54.7 g (0.15 mol) was dissolved in 400 mL of water. With adequate stirring, 26.0 g (0.15 mol) of 1,5,8,12-tetraazadodecane was added. The resulting red–brown solution was cooled to 5 °C in an ice bath, after which 22.5 mL of 40% glyoxal was added with stirring. The reaction mixture was brought to room temperature and allowed to stand for 4 h. The solution was then cooled again to 5 °C and treated with 11.0 g (0.3 mol) of sodium tetrahydroborate in small portions over a 1-h period. After complete addition of the tetrahydroborate, the solution was heated to 90 °C for 30 min and filtered while hot. The obtained Ni(cyclam) complex solution was transferred to a single-necked round flask, and 29.0 g (0.6 mol) of sodium cyanide was added. The mixture was then refluxed for 2 h, and sodium hydroxide (15.0 g, 0.375 mol) was added to the cooled mixture. After evaporation of water on a rotary evaporator until semisolids remained, chloroform was used to extract the free base cyclam [21].

2.2. Catalyst preparation

2.2.1. Chloropropyl-functionalized SBA-15

In a typical synthesis, 16.0 g of 10% (w/w) aqueous solution of P123 was poured into 26.6 g of distilled water, and 4.47 g of sodium metasilicate was added under stirring to yield a clear solution. To this solution, 0.2 g of CPTS (with a silica-to-chloro molar ratio of 20) was added. The mixture was vigorously stirred using a mechanical stirrer at 40 °C until a homogeneous solution was obtained. Then 13.0 g of concentrated hydrochloric acid (37.6%) was quickly added into the solution. The final mixture was aged under stirring for 1 h at 40 °C to get the reactive gel before moving to the microwave digestion system (CEM Corporation, MARS-5). The molar composition of the gel mixture was as follows: $1SiO_2$: 0.05CPTS:0.018P123:11HCl:$117.1H_2O$. The microwave condition for crystallization was set under static conditions at 100 °C for 2 h at an operating power of 300 W (100%). The crystallized product was filtered, washed with warm distilled water, and dried at 80 °C. The surfactant was then selectively removed by Soxhlet extraction with acidified ethanol (2 g concentrated HCl into 100 g EtOH for ca. 0.5 g sample) for 24 h [22].

2.2.2. Cobalt cyclam-functionalized SBA-15 [Co(III)-SBA-15]

The Co(III)-SBA-15 was prepared by encapsulating Co(III) into a cavity of cyclam that was tethered onto the SBA-15 surface via the substitution reaction of the chloro groups of Clpr-SBA-15. Tethering of cyclam and Co(III) encapsulation were carried out according to the following procedure. A mixture of cyclam (0.5 g, 2.5 mmol), Clpr-SBA-15 (1.0 g) in 90 mL of acetonitrile, and triethylamine (1.1 g, 10.9 mmol) was refluxed at 90 °C under stirring for 2 days. The resulting white solid was quantitatively recovered by filtration and washed five times with hot chloroform and three times with hot ethanol. The excess cyclam was removed by Soxhlet extraction over ethanol for 24 h. After drying under vacuum at 100 °C for 24 h, the resulting cyclam-functionalized SBA-15 (cyclam-SBA-15) was dispersed into 90 mL of an ethanolic solution of 0.5 g $CoCl_2 \cdot 6H_2O$ and refluxed for 12 h. During this process, the reaction mixture was constantly bubbled with air to oxidize the Co(II)cyclam to Co(III)cyclam complex to yield Co(III)-SBA-15. The final pale-green Co(III)-SBA-15 was recovered by filtration and washed three times with ethanol, water, and 2 mol L^{-1} HCl so-

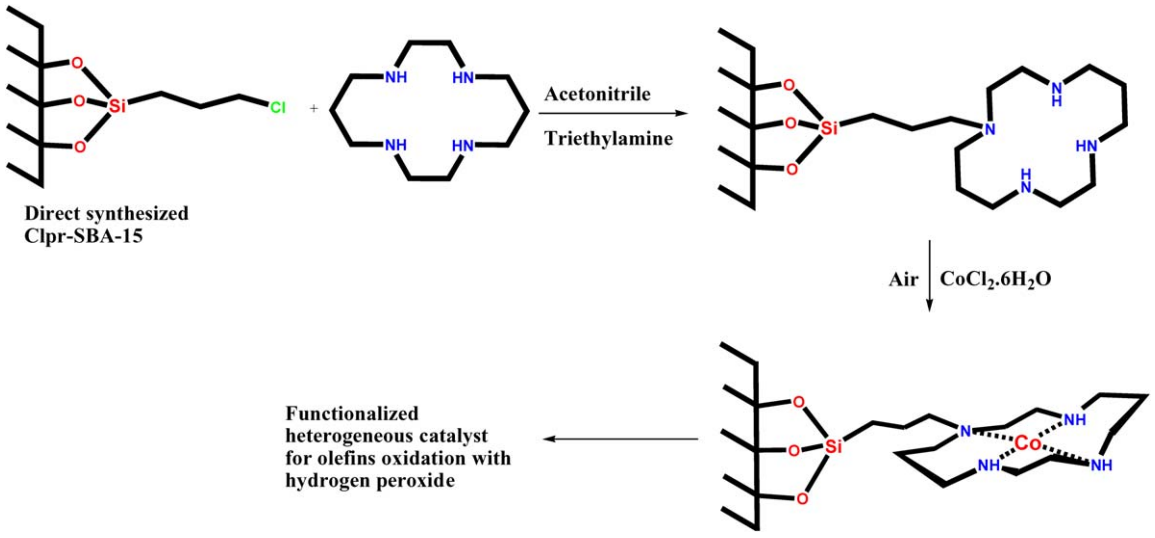

Scheme 1.

lution consecutively and dried under vacuum at 100 °C for 24 h (Scheme 1). Atomic absorption spectroscopy analysis showed that the Co loading was 0.40 mmol g^{-1} of catalyst.

2.3. Catalyst characterization

The obtained materials were characterized by several spectroscopic techniques to confirm the functionality. The structure and crystallinity of the materials were determined using powder X-ray diffraction (XRD) patterns obtained on a Rigaku diffractometer using Cu$K\alpha$ radiation ($\lambda = 0.154$ nm). N_2 adsorption–desorption isotherms and pore characterizations were obtained with a Micromeritics ASAP 2020 device at liquid N_2 temperature. Transmission electron microscopy (TEM) images were obtained using a JEM-3011 instrument (JEOL) equipped with a slow-scan CCD camera operating at 300 keV. Scanning electron microscopy (SEM) images were collected with a JEOL 630-F microscope. UV–vis–NIR diffuse reflectance spectra (DRS) were measured with a Solidspec 3700 UV–vis–NIR spectrometer. For analysis, the sample was loaded into a homemade quartz cell and evacuated under vacuum at 150 °C. The NIR spectra were recorded in the reflectance mode at room temperature. The FTIR spectra were recorded using a Nicolet Impact 410 spectrometer over a range of 400–4000 cm^{-1} at various temperatures in a homemade stainless steel IR cell equipped with KBr windows. Elemental analyses were performed with an EA-1110 analyzer (CE Instruments). Thermogravimetric (TG) analyses were carried out on a TGA/SDTA 851 thermal analysis system (Mettler Toledo Co.) at a heating rate of 10 °C min^{-1} under nitrogen atmosphere. The CP/MAS ^{13}C solid-state NMR spectrum was recorded on a Varian Unity-Inova 400 at 100 MHz with a 7-mm CP/MAS probe and a magic spinning frequency of 5 kHz.

2.4. Electrochemical measurements

The electrochemical analysis (cyclic voltammetry (CV)) was performed to check the redox cyclic transformation of Co species in the Co(III)-SBA-15 catalyst-modified carbon paste electrode. The modified carbon paste electrode was prepared by homogeneous mixing of the dispersed graphite powder with Co(III)-SBA-15 catalyst (graphite/catalyst = 10) and subsequently added to 0.25 g of mineral oil in 20 mL of hexane. The final paste was obtained after a slow evaporation of hexane. The modified carbon paste was packed into an electrode body, consisting of a plastic cylindrical tube (8 mm o.d., 6 mm i.d.) equipped with a copper rod serving as an external electric contact. Appropriate packing was achieved by pressing the electrode surface against filter paper. The carbon paste electrode modified with Co(III)-SBA-15 was used as the working electrode, and a platinum wire was used as the auxiliary electrode. The cyclic voltammogram was recorded on a Solartron Electrochemical Interface unit (model SI 1287) and carried out in unstirred $LiClO_4$ solution with a potential sweep rate of 20 mV s^{-1} from −0.55 to 1.1 V versus SCE. Recording was done first from the oxidation step and then from the reduction step at the carbon paste electrode modified with Co(III)-SBA-15.

2.5. Liquid-phase catalytic oxidation of cycloolefins

A typical experimental procedure for liquid-phase oxidation of cycloolefins was conducted over Co(III)-SBA-15. The cycloolefin oxidation was carried out in a 100-mL round-bottomed flask vessel connected to a water condenser and placed in a temperature-equilibrated oil bath. A mixture of 100 mg of catalyst, 10 mmol olefins, 10 mL of acetonitrile, and 10 mmol hydrogen peroxide (35% in water) was introduced to the reaction vessel and heated at 40 °C with constant stirring. Small amounts of the reaction mixture were frequently removed from the reaction vessel, and the reaction products were analyzed using a Donam DS 6200 gas chromatograph equipped with an HP-5 capillary column (0.32 mm × 30 m) and a flame ionization detector. Product identification was done based on gas chromatography (GC) peaks of the authentic compounds and GC–mass spectrometry (GC–MS) analysis. The

conversions were calculated based on the initial amount of the cycloolefins; the selectivity was calculated based on the total amount of products. Owing to the allylic hydroperoxides species could be partially decomposed during the GC analysis; their amounts were calculated based on double analysis of GC, before and after decomposition with the addition of Ph_3P.

3. Results and discussion

3.1. Preparation and characterization of Co(III)-SBA-15

Fig. 1 shows the small-angle XRD patterns of the surfactant-free Clpr-SBA-15, cyclam-SBA-15, and Co(III)-SBA-15. The Clpr-SBA-15 synthesized by microwave-assisted direct synthesis had a very intense diffraction peak at 0.99° 2θ of (100) reflection and two additional peaks with lower intensity at 1.64° and 1.88° 2θ of (110) and (200) reflections, respectively, indicating high ordering and excellent textural uniformity of the material with 2-D hexagonal (P6mm) structure [23,24].

Further evidence of a high-order mesostructure was provided by SEM and TEM images. Fig. 2 shows SEM (a) and TEM (b–d) images of the Clpr-SBA-15. The SEM image revealed a worm-like morphology of typical mesoporous material with a two-dimensional (2-D) hexagonal structure. The TEM images clearly showed that the material had an array of highly ordered 2-D hexagonal structures, similar to those of pure SBA-15 materials [18,25]. This means that the Clpr-SBA-15 with a highly ordered mesostructure could be successfully synthesized by applying microwave-assisted direct synthesis. This is an interesting finding, because the presence of CPTS in the reaction gel might have an adverse effect on nonionic assembly during

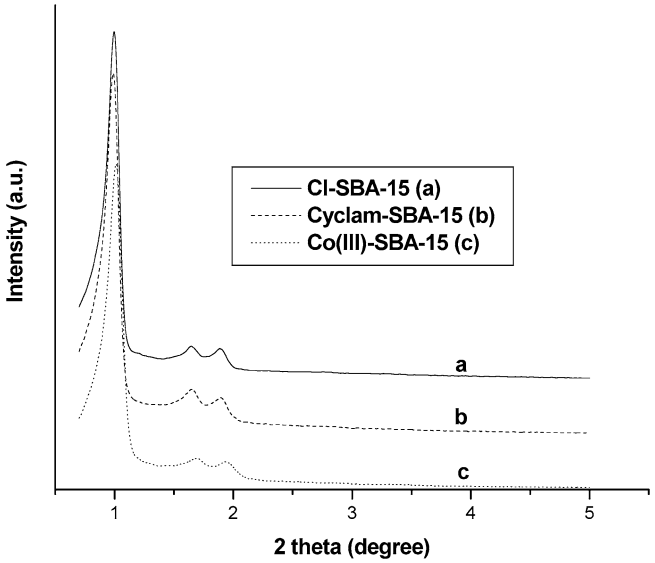

Fig. 1. Small-angle XRD patterns of (a) Clpr-SBA-15, (b) cyclam-SBA-15, and (c) Co(III)-SBA-15.

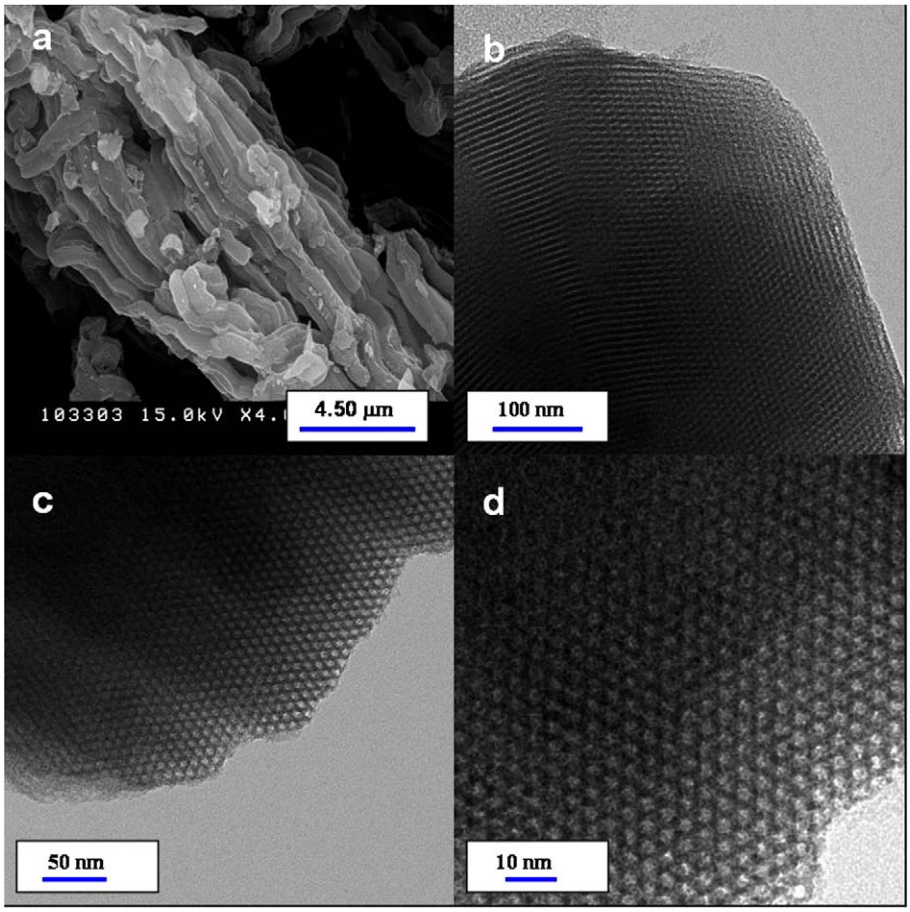

Fig. 2. SEM (a) and TEM (b–d) images of the surfactant-free Clpr-SBA-15 obtained from microwave-assisted direct synthesis.

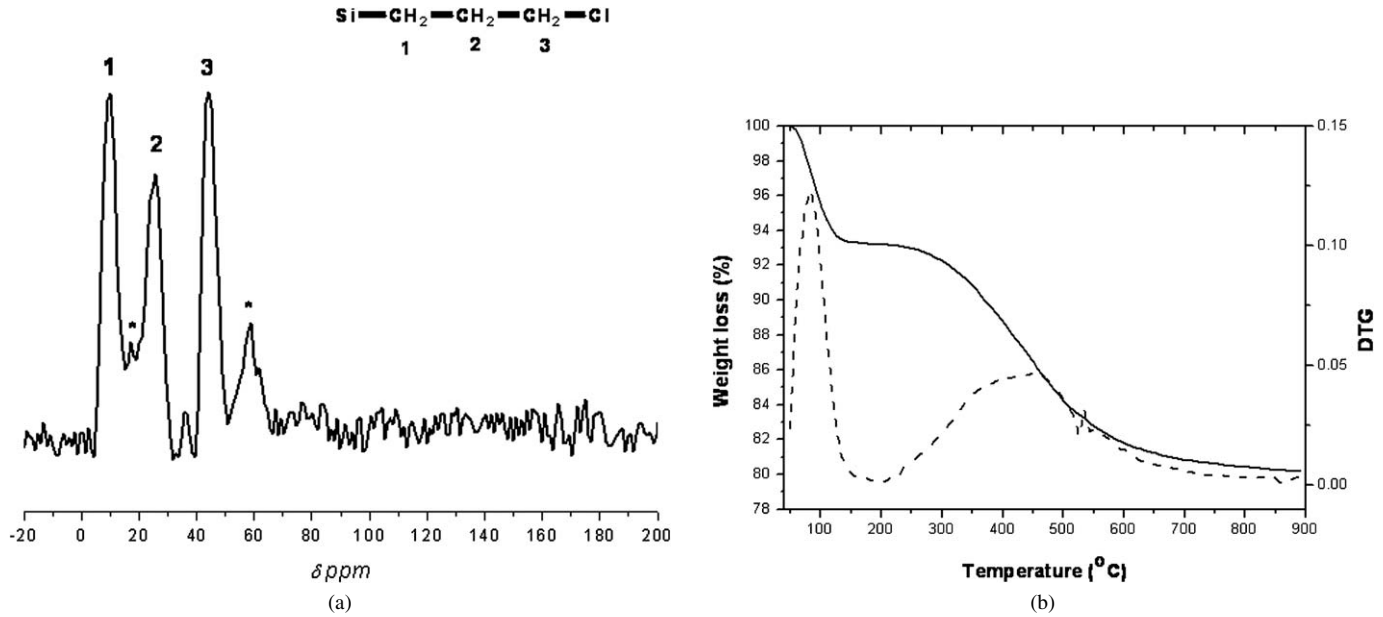

Fig. 3. (a) ^{13}C CP/MAS NMR spectra and (b) TGA and DTG profiles of the surfactant-free Clpr-SBA-15.

direct synthesis and possibly disturb the periodicity and regularity of the resulting materials [12,13,26]. Thus, microwave irradiation was indeed facilitating the supramolecular assembly during the co-condensation process to yield the ordered mesostructure [27–29].

^{13}C solid-state NMR spectroscopy (Fig. 3a) provided clear evidence that the chloropropyl group was indeed functionalized as expected. The ^{13}C CP/MAS NMR spectrum of surfactant-free Clpr-SBA-15 clearly displayed three peaks at 10, 25, and 44 ppm, which were assigned to the C atoms of the tethered chloropropyl group. The asterisks on the peaks at 17 and 58 ppm indicate the residual ethoxy group, which could be due to either incomplete condensation of CPTS or surface reaction during extraction with ethanol [26,30]. The NMR spectrum also confirmed that the chloropropyl moiety was not decomposed during the aging step at high temperature under microwave irradiation. The nearly complete removal of the surfactant could be confirmed with the absence of peaks at 66–77 ppm, corresponding to the P123 surfactant.

The amount of incorporated chloropropyl group was estimated by CHN elemental analysis and TGA techniques. The elemental analysis showed that the amount of tethered chloropropyl group was close to the calculated valued, based on the CPTS concentration in the initial reaction mixture. This means that all of the CPTS in the initial reaction mixture could be effectively incorporated onto SBA-15. The experimental value was 0.88 mmol g^{-1}, slightly larger than the theoretical value of 0.79 mmol g^{-1}. The TGA spectrum of the surfactant-free Clpr-SBA-15 is illustrated in Fig. 3b. The 7% weight loss at temperatures below 100 °C was attributed to the loss of adsorbed water. The weight loss at 250–500 °C can be attributed mainly to the decomposition of chloropropyl groups. The amount of tethered chloropropyl group (∼8%), based on the weight loss in the TGA analysis, was also larger than the theoretical value (∼7%). This discrepancy might be caused by the remaining unincorporated ethoxy group of CPTS and unremoved surfactant residue. In TGA analysis, it also could be caused by the condensation of silanol groups, which occurred in a similar temperature range as for the decomposition of chloropropyl groups [31].

The small-angle XRD patterns of cyclam-SBA-15 (Fig. 1b) and Co(III)-SBA-15 (Fig. 1c) obtained by the chemical modification were very similar to that of the parent Clpr-SBA-15. All XRD patterns exhibited a very intense diffraction peak of (100) and two weak peaks at higher degrees of (110) and (200) refractions at 0.98°, 1.65°, and 1.90° for cyclam-SBA-15 and at 1.0°, 1.70°, and 1.95° for Co(cyclam)-SBA-15, which are characteristic of a 2-D hexagonal (P6mm) structure. This means that the highly ordered mesostructure was maintained during the entire chemical transformation process.

Fig. 4a shows the N_2 adsorption–desorption isotherms of Clpr-SBA-15, cyclam-SBA-15, and Co(III)-SBA-15. All of the samples exhibited well-defined type IV isotherms with H1-type hysteresis loops, characteristic of mesoporous materials with cylindrical-type mesostructures that facilitate the condensation of N_2. The sharp increase in the adsorption step between relative pressures (P/P_0) of 0.6 and 0.8 indicated that the obtained materials had large mesopores with narrow pore size distributions. The lattice parameters and physicochemical characteristics are listed in Table 1. The lattice parameters were calculated from d spacing in the SAXRD patterns. Pore size distributions, pore volumes, and BET surface areas were obtained from analysis of N_2 adsorption–desorption data. The Clpr-SBA-15 had a large mean pore size of 5.1 nm, which could be accessible and substituted by cyclam. The resulting cyclam-SBA-15 and Co(III)-SBA-15 had mean pore sizes of 4.8 and 4.6 nm, respectively (Fig. 4b). The BET surface area of Clpr-SBA-15 was 702 m^2 g^{-1}, which was rather high for a functionalized mesoporous material. However, the BET surface area was significantly reduced to 364 and 358 m^2 g^{-1}, respectively, due to the presence of a significant amount of the

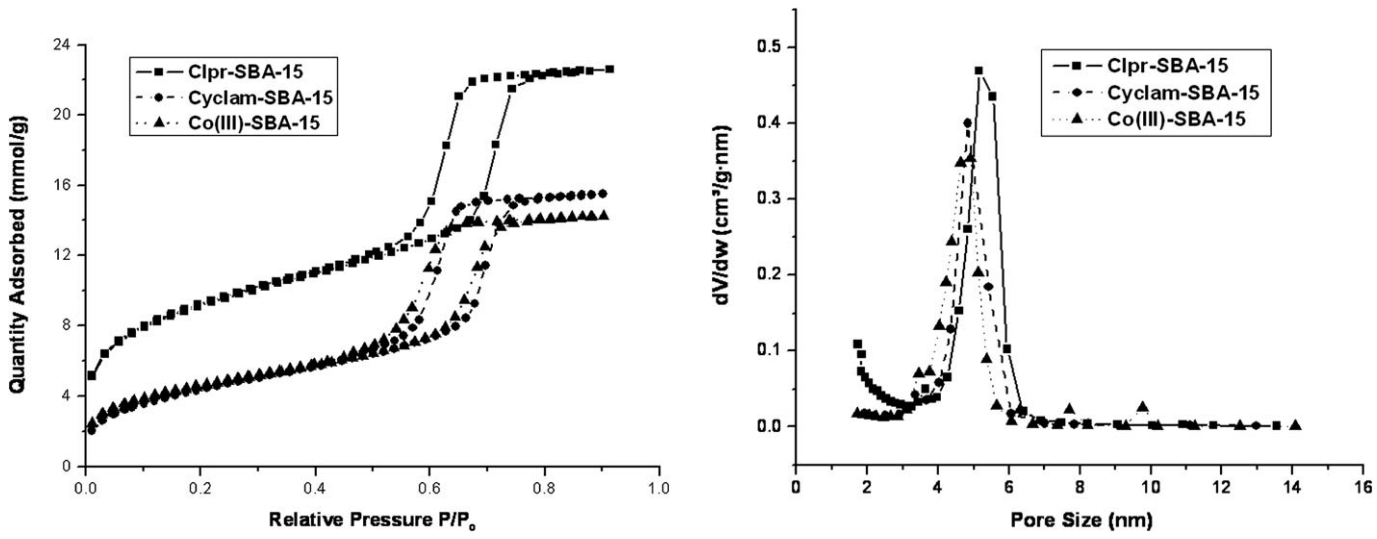

Fig. 4. (a) Nitrogen adsorption–desorption full isotherms for Clpr-SBA-15, cyclam-SBA-15, and Co(III)-SBA-15. (b) Pore distributions for Clpr-SBA-15, cyclam-SBA-15, and Co(III)-SBA-15.

Table 1
Lattice parameter and physicochemical properties of the catalyst

Sample	$d/100$	S_{BET} ($m^2\,g^{-1}$)	Pore volume ($cm^3\,g^{-1}$)	Pore size[a] (nm)
Clpr-SBA-15	89.1	702	0.75	5.13
Cyclam-SBA-15	89.6	364	0.54	4.80
Co(III)-SBA-15	87.4	358	0.49	4.60

[a] Pore size distributions were calculated from the desorption branch by using BJH method.

anchored bulky cyclam and Co(III)cyclam complex inside the mesopores [26,32].

Successful functionalization of the chloropropyl groups onto the SBA-15 mesoporous material through the microwave-assisted direct synthesis, as well as its chemical transformation into cyclam-SBA-15 and Co(III)-SBA-15, were also traced by NIR and IR spectra. Bands at the NIR spectra were generally associated with the harmonic overtones of fundamental and combination bands associated with hydrogen atoms; consequently, they are typically well isolated. This is why the NIR spectra are favored in the analysis of compounds containing O–H, N–H, and/or C–H bonds. Fig. 5 shows the NIR spectra of Clpr-SBA-15, cyclam-SBA-15, and Co(III)-SBA-15. The NIR spectra of Clpr-SBA-15 (Fig. 5a) showed three strong bands at around 2214, 1900, and 1370 nm, corresponding to the vibration transitions of surface hydroxyl groups. The former two bands could be assigned to the combination ($\nu + \delta$) band of stretching (ν) and bending (δ) modes of the nonbonded and bonded surface silanol groups of the SBA-15 material, and the latter was due to the overtone (2ν) absorption band of the stretching (ν) of silanol groups [33,34]. Adsorption bands at 1896, 1950 (as a shoulder), and 1456 nm (as a shoulder) could be assigned to the adsorbed H_2O on the SBA-15 surface. Absorption bands at around 2265–2350 and 1723 nm appeared as assigned to the combination ($\nu + \delta$) band of the CH_2 moiety stretching vibration (ν) and bending (δ) modes and the first overtone band of CH_2 moiety stretching vibration, respectively. The chemical transformation of chloro groups with cyclam was confirmed with the appearance of the absorption band for the secondary amine of cyclam at 1550 nm [35,36]. The higher intensity and area of the CH_2 reflectance band (at 2265–2350 and 1723 nm; Fig. 5a) also indicated the addition of CH_2 moiety on the substitution of cyclam for Cl. The NIR spectra of Co(III)-SBA-15 were found to be similar to those of the cyclam-SBA-15. This means that the structure of tethered cyclam did not change during the cobalt metallation reaction, which was carried out in an ethanolic solution with continuous air bubbling to oxidize the Co(II)cyclam to the Co(III)cyclam complex.

The Co(III)-SBA-15 was analyzed by FTIR at an elevated temperature to check the thermal stability of the fully functionalized SBA-15. It was found that the Co(III)-SBA-15 catalyst had high thermal stability up to at least 250 °C; the vibration bands for the NH and CH_2 stretching at 2800–3400 cm^{-1} were still maintained on heating at 250 °C for 30 min (Fig. 5b).

The Co(III)-SBA-15 catalyst showed three absorption peaks at UV–vis regions of 659, 485, and 260 nm for $^1T_{1g} \leftarrow {}^1A_{1g}$, $^1T_{2g} \leftarrow {}^1A_{1g}$, and ligand to metal charge transfer (LMCT) electronic transition, respectively, which could be attributed to electronic transitions of trans dichloro Co(III)cyclam complex (Fig. 6a) [19]. A slight shift in the lambda maximum of the absorption peaks was observed for the grafted Co(cyclam) compared with homogeneous Co(cyclam) complex in acetonitrile (Fig. 7a). This might be due to the site isolation of the grafted Co(cyclam), which decreased the likelihood of dimer formation by interacting with one another as in the homogeneous Co(cyclam) complex in solution [37].

To study the redox behavior of the entrapped Co species in the Co(cyclam)-functionalized SBA-15, cyclic voltammetry analysis was conducted in unstirred $LiClO_4$ solution in acetonitrile at a potential sweep rate of 20 mV s^{-1} from −0.55 to 1.1 V versus SCE. The oxidation step was recorded first, followed by the reduction step at a carbon paste electrode modified with

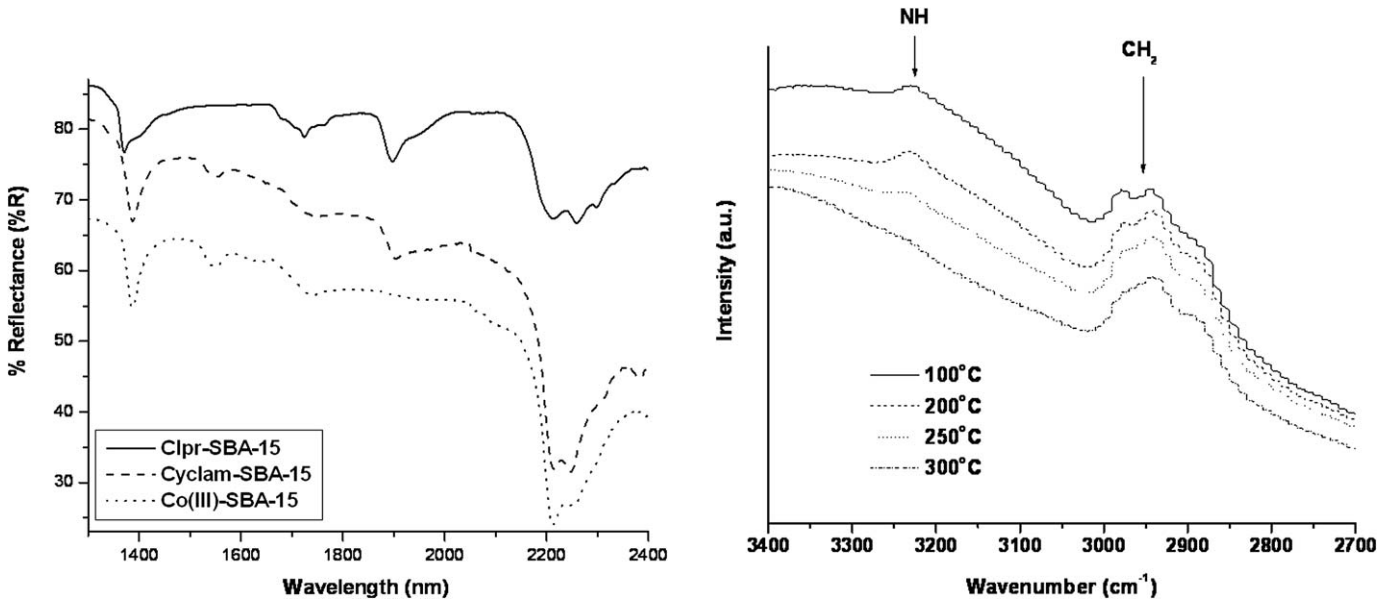

Fig. 5. (a) NIR spectra of Cl-SBA-15, cyclam-SBA-15, and Co(III)-SBA-15 and (b) FTIR spectra of Co(III)-SBA-15 measured after heated at different temperature for 30 min.

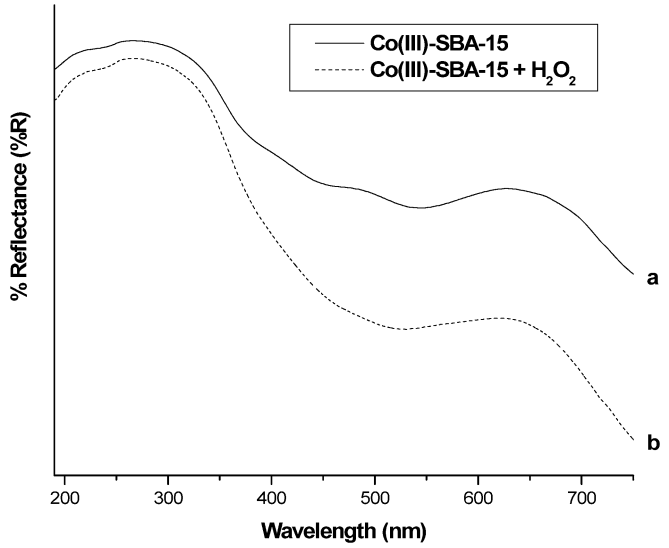

Fig. 6. UV–vis spectra of Co(III)-SBA-15 (a) before and (b) after exposure with H_2O_2.

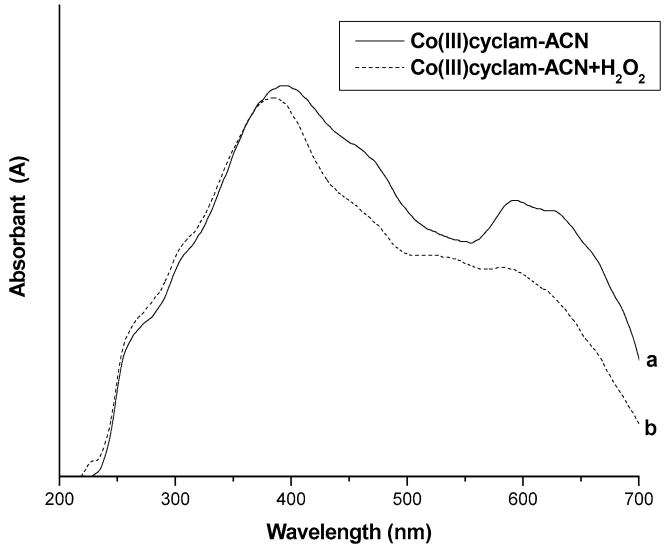

Fig. 7. UV–vis spectra of Co(cyclam) in acetonitrile solution (a) before and (b) after exposure with H_2O_2.

Co(III)-SBA-15. The cyclic voltammogram of carbon paste electrode modified with Co(III)-SBA-15 in 0.1 M $LiClO_4$ solution in acetonitrile showed two reversible redox peaks at −0.16 and 0.42 V versus SCE, corresponding to the Co(II)/Co(III) and Co(III)/Co(II) couples, respectively (Fig. 8) [38]. These reversible changes of Co oxidation states are important in the catalytic oxidation of hydrocarbons involving molecular oxygen, hydrogen peroxide, or organic peroxide.

3.2. Oxidation of cycloolefins

The cobalt-catalyzed oxidation of cycloolefins with hydrogen peroxide can promote either the oxidation of the double bond to produce epoxides or the allylic oxidation leading to allylic hydroperoxides [39]. In the oxidation of cycloolefins with H_2O_2 over Co(III)-SBA-15, the main products were the corresponding allylic hydroperoxides, implying that the oxidation reactions occurred via the allylic substitution mechanism of allylic oxidation. As pointed out by Kochi et al. [17,40], in this allylic oxidation pathway, the Co(cyclam) readily undergoes a 1-electron redox process. Allylic hydroperoxide formation is believed to involve a Co-hydroperoxo complex in the C–OOH bond-forming step [41,42]. The ligand transfer of the metal-bound peroxide to carbon-centered radical forms the allylic hydroperoxide and regenerates the metal catalyst [43]. The allylic oxidation of olefins holds a venerable position in organic synthesis with the possibility of regioselective functionalization

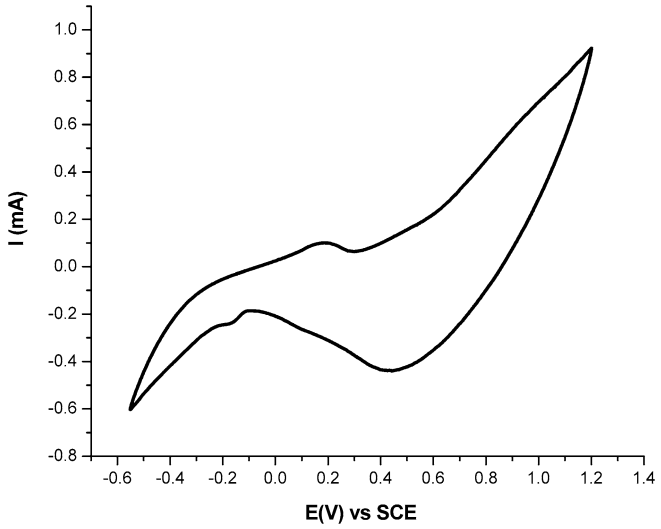

Fig. 8. Cyclic voltammogram of the carbon paste electrode modified with Co(III)-SBA-15.

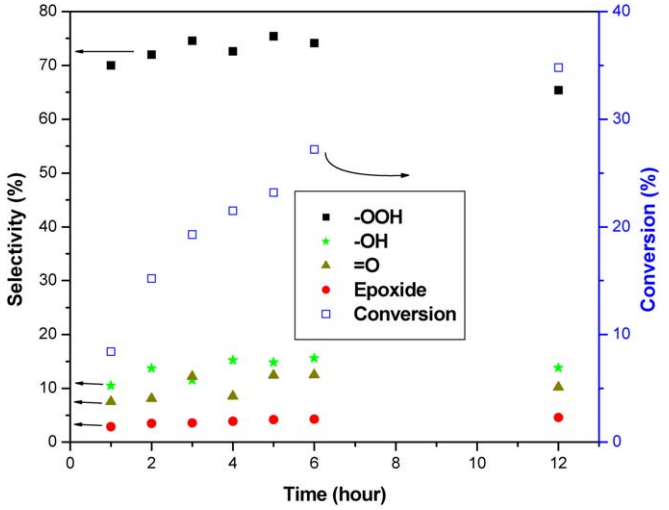

Fig. 9. Conversion and products distribution in the cyclohexene oxidation with H_2O_2 over Co(III)-SBA-15 catalyst.

Table 2
Products distribution of olefins oxidation with hydrogen peroxide over Co(III)-SBA-15

Substrate	Time (h)	Conversion (%)	Product distribution (%)				
			–OOH	–OH	=O	Epoxide	Others
Cyclopentene	6	36.6	72.0	6.8	10.1	9.0	2.1
	12	40.3	48.1	13.8	14.0	18.1	6.0
Cyclohexene	6	27.2	71.1	13.6	10.5	4.0	1.1
	12	34.8	65.4	13.8	10.2	4.6	6.0
Cycloheptene	6	15.9	65.8	4.8	14.0	14.2	1.9
	12	26.9	44.3	4.0	18.2	22.2	11.3

of an allylic C–H bond with oxygen. The allylic peroxides are particularly important in the direct synthesis of allylic alcohols, enones, and enediones from the oxidation of readily available alkenes. They also are important oxygen transfer agents in organic synthesis, for example, in the synthesis of phenol through benzene hydroxylation [44].

Co(III)-SBA-15 has proven to be an affective catalyst in cycloolefin oxidation with hydrogen peroxide as the terminal oxidant to give allylic hydroperoxides as major products. Table 2 shows the product distribution of the cycloolefin oxidation with hydrogen peroxide over the Co(III)-SBA-15 catalyst. The allylic hydroperoxides were the major products, generally exceeding 50% selectivity after 12 h of reaction; other products included the corresponding epoxides, allylic alcohols, and enones. It has been reported that high selectivity of allylic hydroperoxides could not be obtained using molecular oxygen as a terminal oxidant [45–47].

In the presence of the Co(III)-SBA-15, cyclohexene was oxidized to give cyclohexen-1-hydroperoxide (–OOH), 2-cyclohexen-1-ol (–OH), 2-cyclohexen-1-one (C=O), and cyclohexene oxide (epoxide). The product distribution is shown in Table 2 and Fig. 9. As shown in Fig. 9, the selectivity for the (–OOH) exceeded 70% after 1 h and was ca. 65% after 12 h of reaction. This is an interesting observation, because allylic hydroperoxide species are difficult to obtain in such high yields, not only because they are easily decomposed to produce corresponding allyl alcohols and enones, but also because they can act as oxygen-transfer agents for the epoxidation of unreacted olefins in the reaction mixture. Several groups [45–47] have reported that olefins could be oxidized in the presence of metal complex catalysts to yield their hydroperoxide counterparts, however, the selectivities were low.

The major products in cyclopentene and cycloheptene catalytic oxidations with hydrogen peroxide were similar to those of cyclohexene, which gave the hydroperoxide species (–OOH) as the major products. This means that in the cycloolefin oxidation, the hydrogen abstraction mechanism might be preferable as the main pathway in cycloolefin propagation by Co(cyclam)OOH complex. However, with increased reaction time, we observed the decreased selectivity onto (–OOH) species and the increased selectivity for epoxides, which reached up to 18% for cyclopentene oxide and 22% for cycloheptene oxide (Figs. 11 and 12). The epoxides were supposed to be derived mainly from β-hydroperoxyalkyl radicals, obtained through the HOO addition mechanism. The differences in epoxide selectivity based on the cycloolefins can be explained by the differences in the addition/abstraction ratio of the cycloolefins. An earlier study by Kochi and Sheldon [17] found that the ratio of addition to abstraction was strongly dependent on the structure of the cycloolefins, the ratio of which was cyclohexene < cyclopentene < cycloheptene. In good agreement with those studies, our results showed that the selectivities to epoxides followed the order cyclohexane oxide < cyclopentane oxide < cycloheptene oxide.

3.3. Redox and catalytic behavior of Co(III)-SBA-15

The catalysis reaction results showed enhanced catalytic activity for the heterogeneous Co(III)-SBA-15 catalyst compared with the homogeneous Co(cyclam) catalyst in cyclohexene oxidation (Figs. 9 and 10). It is known that in the homogeneous

solution, metallo–amine complexes readily form peroxo, bridging dinuclear complexes with hydrogen peroxide or molecular oxygen [37]. These dinuclear complexes were responsible for the catalase activity of the catalysts in the decomposition of hydrogen peroxide into H_2O and O_2. In the heterogeneous system, where the metal complexes were tethered and isolated, the catalase active dinuclear complexes could not be formed on the surface of support. Hence, the immobilized Co(cyclam) onto SBA-15 could more effectively activate the H_2O_2 for the cyclohexene oxidation.

This phenomenon is supported by the changes in the UV–vis spectra of Co(III)-SBA-15 and homogeneous Co(cyclam) complex solution after treatment with H_2O_2. The electronic spectra of Co(III)-SBA-15 after treatment with aqueous hydrogen peroxide solution in ethanolic solution showed a complete disappearance of the peak at 485 nm for the $^1T_{2g} \leftarrow {}^1A_{1g}$ transition and an increased extinction coefficient (ε) for the $^1T_{1g} \leftarrow {}^1A_{1g}$ transition peak at 659 nm. This change in the electronic transition can be attributed to the structural change of the Co(cyclam) complex caused by the hydroperoxo species bounding at its axial coordination site through activation with H_2O_2 (Fig. 6b). For comparison, Co(III)N_4O-type complexes also gave two peaks similar to the hydrogen peroxide-treated Co(III)-SBA-15 [48]. However, different changes in the UV–vis spectra were observed for the homogeneous solution of Co(cyclam) complex in acetonitrile solution after the reaction with hydrogen peroxide. These spectra showed a decreased extinction coefficient (ε) for the $^1T_{2g} \leftarrow {}^1A_{1g}$ and $^1T_{1g} \leftarrow {}^1A_{1g}$ transitions and the appearance of new absorption band at 538 nm, which could be attributed to the formation of hydroperoxo complex and bis-μ-oxo dimeric complex, respectively (Fig. 7b).

Thus, the anchored Co(cyclam) complex activated the hydrogen peroxide to generate hydroperoxide products through allylic oxidation of the cycloolefins. The redox reaction of cycloolefin substrates with the Co(III)-SBA-15 proceeded through a one-equivalent change in the oxidation state of the Co(III) to Co(II), generating a HOO· free-radical intermediate. The resulting Co(II) species subsequently form a complex with the resulting HOO· through the formation of Co(III) hydroperoxo complex, facilitating the reaction between cycloolefins and the HOO·.

The reaction between the resulting Co(cyclam)OOH complex and the cycloolefins could occur via two routes, hydrogen abstraction and hydroperoxy radical addition to the double bond, producing allylic radicals and β-hydroperoxyalkyl radicals, respectively. The allylic radicals reacted with the Co(cyclam)OOH complexes to yield allylic hydroperoxides, whereas the β-hydroperoxyalkyl radicals followed by the unimolecular decomposition gave epoxides and hydroxyl radicals.

Attempts to reuse our catalyst for a second run after collecting the catalyst in the end of the first run were not successful. The ligand decomposition, which in turn caused catalyst degradation, was supposed to be responsible for this deactivation. The homolytic cleavage of the metal hydroperoxo active intermediate, M–O–O–H, is known to generate an indiscriminate free hydroxyl radical oxidant, which could attack most of the ligands [49]. The observed UV–vis spectra showed the detri-

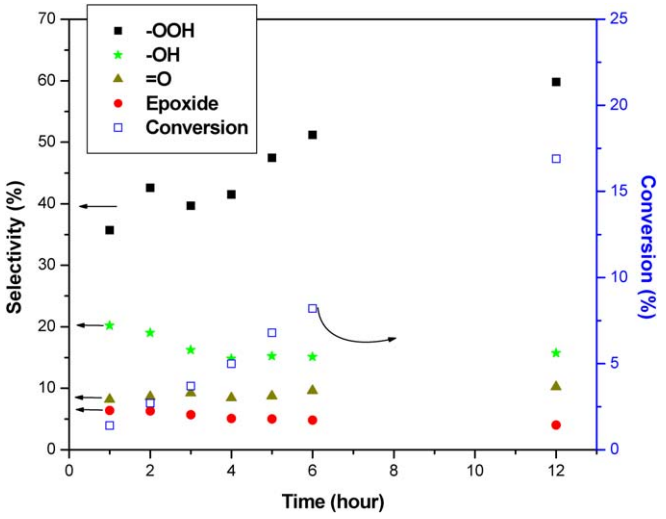

Fig. 10. Conversion and products distribution in the cyclohexene oxidation with H_2O_2 using Co(cyclam) as homogeneous catalyst.

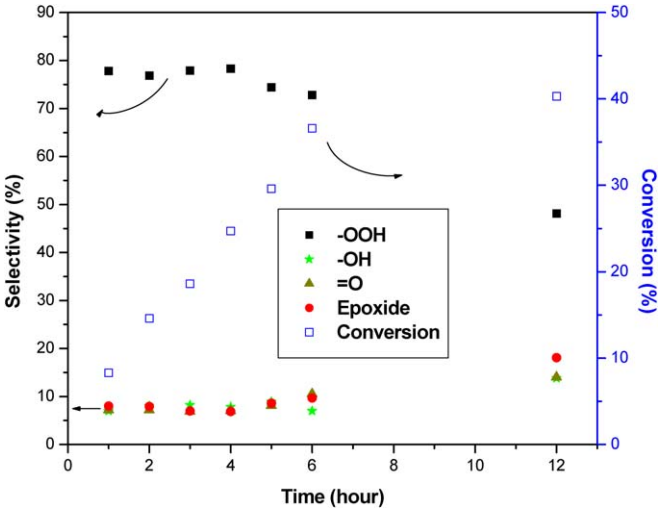

Fig. 11. Conversion and products distribution in the cyclopentene oxidation with H_2O_2 over Co(III)-SBA-15 catalyst.

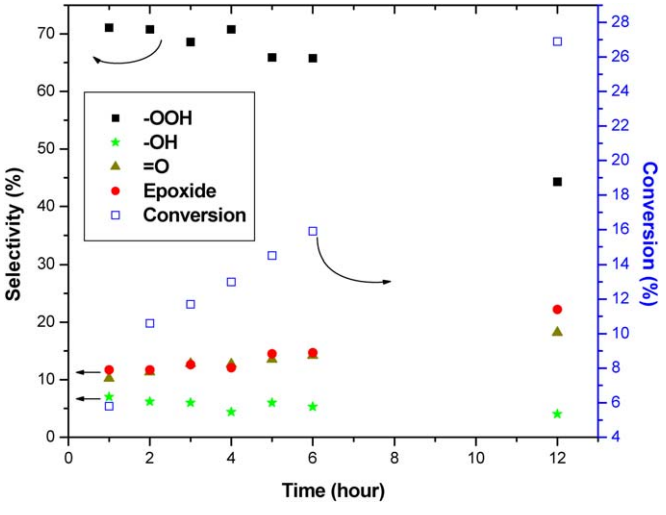

Fig. 12. Conversion and products distribution in the cycloheptene oxidation with H_2O_2 over Co(III)-SBA-15 catalyst.

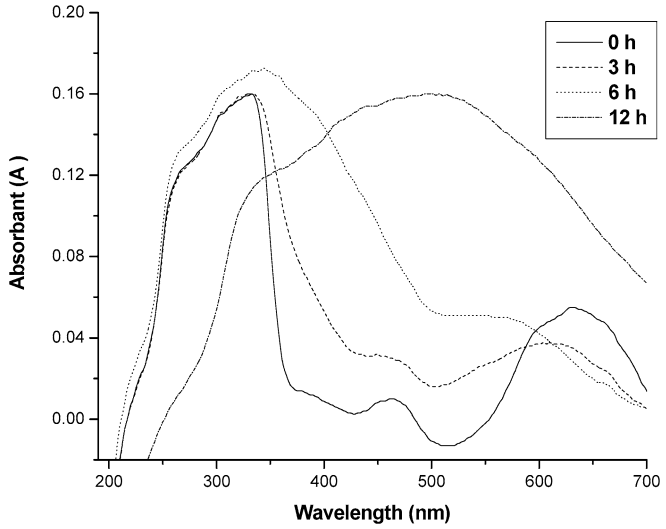

Fig. 13. UV–vis spectra of Co(cyclam) complex in homogeneous catalysis of cyclohexene with H_2O_2 depend on time.

mental degradation of the Co(cyclam) catalyst in the homogeneous reaction after a long reaction period (Fig. 13). A similar degradation process was believed to occur in this heterogeneous catalytic system, thus deactivating the catalyst. Investigations on suppressing the homolytic cleavage to prevent catalyst degradation are currently underway.

4. Conclusion

Co(III) was successfully functionalized onto SBA-15 mesoporous silica by encapsulating within the macrocycle cavity (in this case, cyclam) after the substitution reaction of chloropropyl functionalized the SBA-15 mesoporous silica. The reversible oxidation–reduction process of the Co species played an important role in initiating the catalytic oxidation of olefins. The Co(III)-SBA-15 catalyzed the oxidation of cyclopentene, cyclohexene, and cycloheptene mainly through the allylic substitution mechanism to produce corresponding allylic hydroperoxides as major products. Because allylic hydroperoxides are important intermediates and widely used oxygen-transfer agents in epoxidation and hydroxylation, our interesting results can be applied to the coupled oxidation system with multi-substrates in one pot using in situ-generated allylic hydroperoxide as an oxygen-transfer agent to oxidize stable hydrocarbons.

Acknowledgments

This work was supported by the Korean Industry and Energy Ministry of Commerce (10023056-2005-21) and the Ministry of the Environment (2005-03001-0020-0).

References

[1] A. Corma, Chem. Rev. 97 (1997) 2373.
[2] J.Y. Ying, C.P. Mehnert, M.S. Wong, Angew. Chem. Int. Ed. 38 (1999) 56.
[3] A. Stein, B.J. Melde, R.C. Schroden, Adv. Mater. 12 (2000) 1403.
[4] J.-S. Chang, J.S. Hwang, S.-E. Park, Res. Chem. Intermed. 29 (2003) 921.
[5] I.W.C.E. Arent, R.A. Sheldon, Appl. Catal. A 212 (2001) 175.
[6] J.M. Kim, J.H. Kwak, S. Jun, R. Ryoo, J. Phys. Chem. 99 (1995) 16742.
[7] S. Wu, Y. Han, Y.-C. Zou, J.-W. Song, L. Zhao, Y. Di, S.-Z. Liu, F.-S. Xio, Chem. Mater. 16 (2004) 486.
[8] Y. Li, Z. Feng, Y. Lian, K. Sun, L.L. Zhang, G. Jia, Q. Yang, C. Li, Micropor. Mesopor. Mater. 84 (2005) 41.
[9] G. Kickelbick, Angew. Chem. Int. Ed. 43 (2004) 3102.
[10] T. Yokoi, H. Yoshitake, T. Yamada, Y. Kubota, T. Tatsumi, J. Mater. Chem. 16 (2006) 1125.
[11] J.H. Clark, D.C. Macquarrie, Chem. Commun. (1998) 853.
[12] R.J.P. Corriu, A. Mehdi, C. Reye, J. Mater. Chem. 15 (2005) 4285.
[13] A.S.M. Chong, X.S. Zhoa, J. Phys. Chem. B 107 (2003) 12650.
[14] M. Hartmann, L. Keven, Chem. Rev. 99 (1999) 635.
[15] B.K. Das, J.H. Clark, Chem. Commun. (2000) 605.
[16] D.R. Burri, K.-W. Jun, Y.-H. Kim, J.M. Kim, S.-E. Park, J.S. Yoo, Chem. Lett. 31 (2002) 212.
[17] R.A. Sheldon, J.K. Kochi, Metal-Catalyzed Oxidation of Organic Compounds, Academic, New York, 1981.
[18] L.F. Lindoy, The Chemistry of Macrocyclic Ligand Complexes, Cambridge Univ. Press, Cambridge, 1989.
[19] B. Bosnich, C.K. Poon, M.L. Tobe, Inorg. Chem. 4 (1965) 1102.
[20] S.-C. Han, Sujandi, S.-E. Park, Bull. Korean Chem. Soc. 26 (2005) 1381.
[21] E.K. Barefield, F. Wagner, A.W. Herlinger, A.R. Dahl, in: F. Basolo (Ed.), Inorganic Synthesis, vol. 16, McGraw–Hill, New York, 1976, p. 220.
[22] W.J. Hunks, G.A. Ozin, Adv. Func. Mater. 15 (2005) 259.
[23] D. Zhao, Q. Huo, J. Feng, B.F. Chmelka, G.D. Stucky, J. Am. Chem. Soc. 120 (1998) 6024.
[24] J.M. Kim, G.D. Stucky, Chem. Commun. (2000) 1159.
[25] A.P. Wight, M.E. Davis, Chem. Rev. 102 (2002) 3589.
[26] R.J.P. Corriu, A. Mehdi, C. Reyé, C. Thieuleux, Chem. Mater. 16 (2004) 159.
[27] S.-E. Park, J.-S. Chang, Y.K. Hwang, D.S. Kim, S.H. Jhung, J.S. Hwang, Catal. Surv. Asia 8 (2004) 91.
[28] Y.K. Hwang, J.-S. Chang, Y.-U. Kwon, S.-E. Park, Micropor. Mesopor. Mater. 68 (2004) 21.
[29] Y.K. Hwang, J.-S. Chang, S.-E. Park, D.S. Kim, Y.-U. Kwon, S.H. Jhung, J.-S. Hwang, M.S. Park, Angew. Chem. Int. Ed. 44 (2005) 556.
[30] K. Cassiers, P. Van Der Voort, E.F. Vansant, Chem. Commun. (2000) 2489.
[31] X. Wang, K.S.K. Lin, J.C.C. Chan, S. Cheng, J. Phys. Chem. B 109 (2005) 1763.
[32] R.I. Kureshy, I. Ahmad, N.H. Khan, S.H.R. Abdi, K. Pathak, R.V. Jasra, J. Catal. 238 (2006) 134.
[33] M. Takeuchi, G. Martra, S. Coluccia, M. Anpo, J. Phys. Chem. B 109 (2005) 7387.
[34] M. Takeuchi, K. Sakamoto, G. Martra, S. Coluccia, M. Anpo, J. Phys. Chem. B 109 (2005) 15422.
[35] L. Xu, H. Fu, J.R. Schlup, J. Am. Chem. Soc. 116 (1994) 2821.
[36] J. Mijovic, S. Andjeli, Macromolecules 28 (1995) 2787.
[37] T.H. Bennur, D. Srinivas, S. Sivasanker, J. Mol. Catal. Chem. 207 (2004) 163.
[38] E. Simon, P. L'Haridon, R. Pichon, M. L'Her, Inorg. Chim. Acta 282 (1998) 173.
[39] J.D. Koola, J.K. Kochi, J. Org. Chem. 52 (1987) 4545.
[40] K. Srinivasan, S. Perrier, J.K. Kochi, J. Mol. Catal. 36 (1986) 297.
[41] J. Eaes, M. Watkinson, Angew. Chem. Int. Ed. 40 (2001) 3567.
[42] D.E. Hamilton, R.S. Drago, A. Zombeck, J. Am. Chem. Soc. 109 (1987) 374.
[43] A.J. Catino, R.E. Forslund, M.P. Doyle, J. Am. Chem. Soc. 126 (2004) 13622.
[44] A. Fukuoka, K. Fujishima, M. Chiba, A. Yamagishi, S. Inagaki, Y. Fukushima, M. Ichikawa, Catal. Lett. 68 (2004) 241.
[45] R.-M. Wang, C.-J. Hao, Y.-F. He, C.-G. Xia, J.-R. Wang, Y.-P. Wang, J. Appl. Polym. Sci. 75 (2000) 1138.
[46] A. Fukuoka, K. Fujishima, M. Chiba, A. Yamagishi, S. Inagaki, Y. Fukushima, M. Ichikawa, Catal. Lett. 68 (2000) 241.
[47] J.M. Fraile, J.I. García, J.A. Mayoral, E. Vispe, D.R. Brown, M. Naderi, Chem. Commun. (2001) 1510.
[48] C. Hu, R.M. Chin, T.D. Nguyen, K.T. Nguyen, P.S. Wagenknecht, Inorg. Chem. 42 (2003) 7602.
[49] W.R. Sanderson, Pure Appl. Chem. 72 (2000) 1289.